PHILOSOPHICAL TRANSACTIONS OF THE ROYAL SOCIETY A MATHEMATICAL, PHYSICAL & ENGINEERING SCIENCES

Some Consequences of Solar Wind Induction in the Moon

C. P. Sonett

Phil. Trans. R. Soc. Lond. A 1977 **285**, 537-547
doi: 10.1098/rsta.1977.0097

Phil. Trans. R. Soc. Lond. A. **285**, 537–547 (1977) [537]
Printed in Great Britain

Some consequences of solar wind induction in the Moon

By C. P. Sonett
Dept. of Planetary Sciences and Lunar and Planetary Laboratory, University of Arizona, Tucson, Arizona 85721, *U.S.A.*

Experiment shows the Moon to be asymmetrically excited by the solar wind in the classical spherical transverse electric mode. Both the magnetic dipole and quadrupole are noted, corresponding to Mie scattering, with the fields confined to the lunar interior. Leakage out of the antisolar cavity is evanescent below about 50 Hz. The low bulk conductivity of the interior (from inversion of magnetic signals) is two orders lower than for Earth at equivalent depth. This is consistent with a hot interior only if the rock conductivity function has anomalously low activation energy, suggesting low Fe^{3+} content. Extrapolation of the induction and the complementary transverse magnetic mode to the early solar system shows a consistent pattern of heating of the lunar core, surface, and asteroidal parent bodies independently of accretion or radionuclides. Thus fast highland and core formation can take place provided the induction is intensified by rapid solar spin and a pre-main sequence T Tauri-like plasma flow.

1. Introduction

The Moon, like all planets out to at least Jupiter (Wolfe *et al.* 1974), is bathed in the supermagentosonic plasma issuing from the Sun. This forms the lunar 'atmosphere' in which the Moon has been immersed since its beginning. The interplanetary magnetic field which accompanies the solar wind is constantly agitated by waves and discontinuities which excite the Moon, and the dynamic pressure of the solar wind against the Moon provides the unique and critical function of confining the magnetic field induced in the Moon's interior which results in a substantial increase in the signal to noise ratio (s/n) of magnetic echo signals returned from depth and perceived on the surface. The excitation mode in the Moon which has been unequivocally detected is transverse electric (t.e.) which corresponds electromagnetically to the eddy current induction due to the time dependent fluctuations of the forcing magnetic field. The confinement is imperfect because the solar wind pressure is not present on the dark side of the Moon. It is also possible that for frequencies above the ion gyro frequency of the solar wind, ion whistlers are excited on the sunward hemisphere in analogy with the bow shock wave upstream of the Earth. With the possible exception above the ion whistler frequency, there is no true scattered field because of the confinement. A propagated field is ruled out in any event by the restriction to conduction currents, displacement currents being ignored because of the low frequency. Though a radiation field is absent this is not a fundamental restriction and it is entirely possible that a displacement contribution could be present in the outer part of the lunar crust where the bulk electrical conductivity becomes small.

Since the basic wave equations of lunar induction (Schubert & Schwartz 1972) are similar to those encountered in optics, at very low frequency the induction can be regarded as the counterpart of Rayleigh scattering, transforming at higher frequencies where $kR \gtrsim 1$ to Mie scattering, where k is the characteristic wave number in the solar wind and R_M the lunar radius.

Although for 3/4 of the lunar month the Moon is in the solar wind, for the remaining week it moves through the geomagnetic tail. This latter region is divisible into a plasma sheet and tail lobes. In the plasma sheet there exists evidence that the plasma *flow field* is involved in the induction (Schubert *et al.* 1974) but the details are more obscure than in the solar wind. In the tail lobes plasma motions are thought to be substantially below the threshold where the dynamic pressure resulting from the relative motion of plasma and Moon becomes important. There the Moon is viewed as a spherical radiator immersed in a hot stationary (?) plasma excited by a field of plasma waves more regular than in the solar wind (Schubert *et al.* 1975*a*, *b*). It is in the solar wind, its accompanying magnetosheath plasma, and in the tail lobes where induction experiments can best be carried out, though for the tail lobes the theory is not yet formally worked out.

2. The transfer functions

At medium and high frequency (above 10^{-4} Hz) the response of the Moon is most conveniently defined in terms of a strictly empirical transfer function, based upon the fields observed at Explorer 35 and upon the lunar surface at the l.s.m. In the frequency domain

$$A_i(f) = [H_{2i}(f) + H_{1i}(f)]/H_{1i}(f), \tag{1}$$

where $\boldsymbol{A}(f)$ is a vector with components A_i $(i = \hat{x}, \hat{y}, \hat{z})$, $H_{1i}(f)$ and $H_{2i}(f)$ are respectively the power spectral densities of the time series $h_{1i}(t)$ and $h_{2i}(t)$ of the three components of the *interplanetary magnetic field* and the *induced lunar fields* respectively. Thus $A_i(f)\,H_i(f)$ is the total power spectral density of the ith component at frequency, f, on the lunar surface. The current standard coordinate system (ALSEP) consists of a mutually orthogonal set of unit vectors defined by positive x locally normal outward from the surface of the Moon, y positive eastward, and z positive northward (Sonett *et al.* 1972). ALSEP coordinates are based upon the assumption of continuity of the normal component of B across the surface boundary of the Moon and the convenience of a compass related basis for y and z, and also upon spherically symmetric plasma (s.s.p.) (Sonett *et al.* 1972) confinement of the induced magnetic field.

For cases where $A_i(f) \approx 1$ when $f \approx f_0$, it is more convenient for analysis to redefine the lunar response in terms of a true transfer function, called here the *gain function*. It is defined as

$$G_i(f) = H_{2i}(f)/H_{1i}(f) \quad i = x, y, z. \tag{2}$$

Lunar transfer functions derived from Fourier analysis of $h_{1i}(t)$ and $h_{2i}(t)$ are shown in figure 1 where $A_i(f)$ are given in the upper panel for the sunward or day side of the Moon (solid lines) (Sonett *et al.* 1972) and for the diamagnetic cavity (indicated by primes, shaded lines) (Schubert *et al.* 1973). The lower panel shows $A_i(f)$ for the Moon in the geomagnetic tail field. Solid lines indicate component transfer functions for the plasma sheet (Schubert *et al.* 1974) and the shaded lines for tail lobes (Schubert *et al.* 1975*a*, *b*). Transfer functions for all four regions of space show characteristic differences, indicative of quite different plasma regimes, *but in all cases plasma is present in sufficient density to affect the properties of the transfer functions.*

The permanent magnetic field at the Apollo 12 site has been known to be affected by variations of plasma pressure during times of interplanetary disturbance (Dyal *et al.* 1972). Rotation of coordinates of the transfer functions reveals that the direction of maximum response at Apollo 12 is along the direction of the permanent magnetic field (approximately NW–SE) (Sonett *et al.* 1972). Thus it is reasonable to infer that a noise source is seated in the interaction

and contaminates the transfer functions. The assumption of an *incoherent* addition of the induction and interaction sources of field together with the naive assumption that the noise is due to compressive effects generating magnetoacoustic waves, allows the noise source to be isolated; the direction of minimum response measures the true internal induction. This has been carried out defining the 'noise-free' transfer function as $A_{\min}$ and is the basic transfer function used in the conductivity iterations reviewed in the following section (Sonett *et al.* 1972).

However, figure 1 shows the directional asymmetry to be a persistent feature in *all* regions of space, and the permanent field at Apollo 12 is screened from the solar wind both in the cavity and magnetic tail lobes. (Some effect of plasma pressure would be expected in the plasma sheet.) Thus the asymmetry in the transfer functions cannot be wholly explained by solar wind pressure.

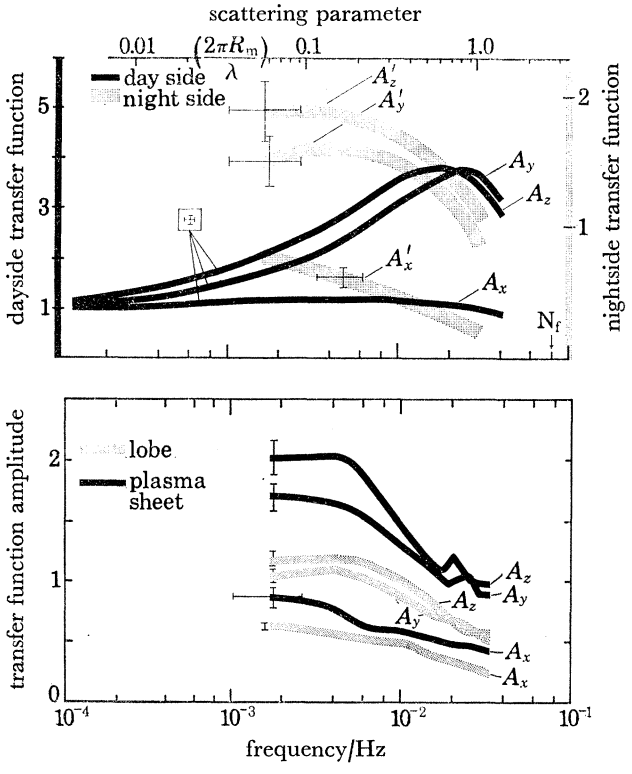

FIGURE 1. Composite lunar transfer functions for the Moon immersed in the solar wind (sunward hemisphere-solid lines; cavity-shaded lines) in the upper panel, and similar data for the Moon in the geomagnetic tail field (lower panel). The latter shows plasma sheet data (solid lines) and tail lobes (shaded lines). The Mie scattering parameter is plotted for the solar wind in the upper abscissa for $V_p = 300$ km/s. (From *Phys. Earth Planet. Int.* **10**, 313, 1975.)

3. BULK ELECTRICAL CONDUCTIVITY PROFILE-PRESENT LIMIT OF RESOLUTION AND COMPARISON BETWEEN MODELS

Both time series transients and Fourier transforms have been used to derive conductivity profiles for the Moon. Figure 2 shows such a set obtained from an iterative inversion on the transfer function, $A_{\min}$ (Sonett *et al.* 1972). Radii are restricted to three layers with conductivity and radii of the layers as free parameters to be determined. Convergence to an acceptable conductivity profile and termination of the iteration is based upon the following technique.

Each data transfer function is characterized by a discrete set of values, $A_k(f_k)$ where $k = 1, 2, \ldots, n$, where n represents the number of significant frequency bands determined by the resolution of the power spectral density (p.s.d.). For each time series, j, a power spectral density and transfer function is determined. For the jth time series, the transfer function at frequency, f_k, is defined as $A_{kj}(f_k)$. The sum $\sum_j A_{kj}(f_k)$ is used to define the final composite transfer function $A_k(f_k)$ and the standard error, $e_k(f_k)$.

In the iterative loop the calculation begins with the assumption of an arbitrary conductivity profile. The calculation determines the differences $\delta_k(f_k)$ between this and A_k for each k, and the profile correspondingly corrected. These differences squared are compared for each iteration with e_k^2, and when $\sum_k \delta_k^2(f_k) \approx \sum_k e_k^2(f_k)$ the iteration is terminated.

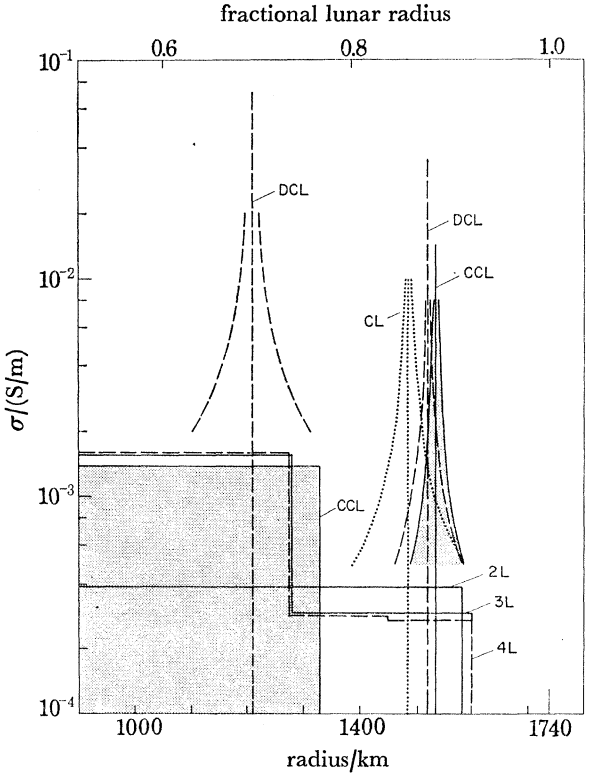

FIGURE 2. Suite of lunar conductivity profiles from inversion of the transfer functions of figure 1. 2L, 3L, and 4L models are two, three, and four layer monotonic respectively; c.c.l. is core plus current layer, c.l. current layer alone, and d.c.l. dual current layer. Models with current layers have an electrical admittance equal to that of the finite layers of the monotonic models. The above represents the s.s.p. resolution limitations. (Adapted from Sonett *et al.* 1972.) (From *Proc. Third Lunar Sci. Conf.*, **3**, 2320, 1972, *Geochim. cosmochim. Acta*, Suppl. 3.)

Limits on resolution and uniqueness are indicated by figure 2 which shows the primary model classes, two layer (2L), three layer (3L), four layer (4L), double current layer (d.c.l.), core plus current layer (c.c.l.), and current layer (c.l.). Permissible models based upon the residual error differences are 3L, 4L, d.c.l., and c.c.l. Data below a depth of about 500–600 km is unreliable. The frequency band used in figure 2 extends from 10^{-4} Hz to $f_{\text{Nyquist}} = 0.04$ Hz. Limitation on resolution is attributed partially to averaging over many scattering angles and to the sun angle dependence of the l.s.m. position. Also the inversion theory here is restricted to spherically

symmetric (s.s.p.) theory making no allowance for cavity fields. About 120 swaths of 1 h length are used in the Fourier transformations.

The procedure outlined above has been applied to various representations of A including A_y and $A_{\min}$ using various values for V_p and θ (figure 3). The results are tabulated in detail in Sonett *et al.* (1972*b*). At intermediate depth in the Moon large variations in V_p and θ cause only moderate changes in the conductivity profile. This may explain the reasonable intermediate depth comparison between time series transient analyses and power spectral density inversions. Differences arise from the likely fundamental differences in the model theories employed in the time cases and to the structure of the two analyses.

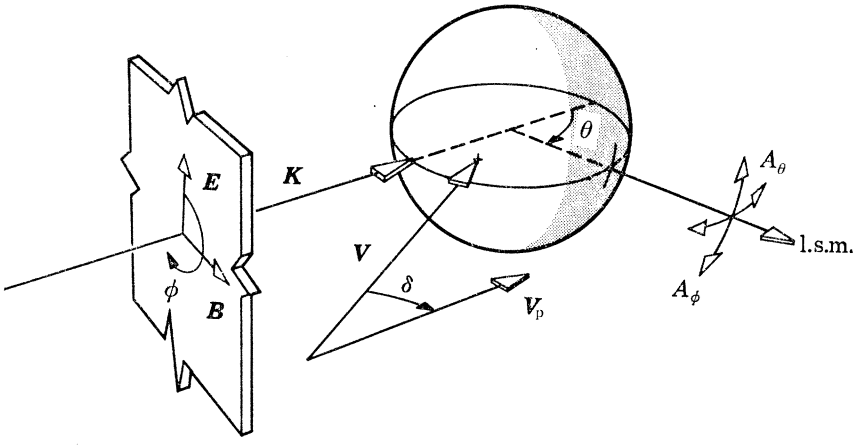

FIGURE 3. Scattering geometry for solar wind plane waves incident upon the Moon. The vector, $\boldsymbol{K}$, defines the wave normal surface (constant phase) while the polarization is measured clockwise looking in the direction of positive $\boldsymbol{k}$ from $\boldsymbol{E}$. $\boldsymbol{V}_s$ is the solar wind bulk velocity vector while $\boldsymbol{V}_p$ is the apparent wave phase velocity, i.e. the speed in the direction of $\boldsymbol{k}$. The scattering angle is measured between $\boldsymbol{K}$ and the local time position of the l.s.m. on the surface of the Moon. A_θ and A_ϕ are the tangential transfer functions measured in coordinates defined by these scattering parameters. (From *Proc. Third Lunar Sci. Conf.*, **3**, 2323, 1972 *Geochim. cosmochim. Acta*, Suppl. 3.)

The level of resolution available from the data used for the p.s.d. inversions does not permit a choice between permissible models. The c.c.l. model as indicated in earlier study (Sonett *et al.* 1971*a*, *b*), suggests a layer of high conductivity matter is present at a depth of about 150–200 km. Electrically the shell in the 3L model may be collapsed into a spike of enhanced conductivity, provided that the total electrical *admittance* of the layer in question is held fixed. This conclusion was confirmed by Schubert & Colburn (1971) who demonstrated the equivalence between a monotonic three layer model derived from time series analysis and c.c.l. model. A precise statement is given by the d.c.l. admittances which define the product σd and its depth for each of two layers, where d is the layer width. Use of a d.c.l. model significantly eases the computational problem in many calculations as the layers are then represented by delta functions. The possible significance of the conductivities found in these models is discussed later in the section on lunar temperature estimates.

A compact comparison of conductivity models and their relation to those for Earth is shown in figure 4 where the lower panel shows the lunar data from several inversions of response into conductivity, corresponding to incident forcing field phase velocities, V_p = 200, 300, and 400 km/s (heavy lines). The figure also shows a transient analysis of Dyal *et al.* (1974) (dashed line), a later transient analysis combining tail lobe and cavity data (dotted line) (Dyal *et al.* 1975), and lastly a Fourier analysis of transients (mixed broken line) (Kuckes 1974). The solid light

line is a conductivity analogue to the Ringwood–Essene solidus (Ringwood & Essene 1970) obtained by using the Red Sea olivine measured by Duba *et al.* (1974) in the laboratory, to change the temperatures of the solidus to an equivalent conductivity. The Sonett *et al.* (1972) data are based upon s.s.p. theory using sunward hemisphere data. Errors are likely from the incomplete correction to signal anisotropy, the Sun angle, V_p, and the effect of averaging over all wave front normal directions for the incoming radiation field. The Dyal *et al.* (1974, 1975; Dyal & Parkin 1973) determinations do not take into account higher order modes; and cavity and tail lobe data is mixed with the assumption that the lunar neighbourhood is vacuum. Signal anisotropy is not considered in the transient analysis so no direct comparison can be made with the p.s.d. use of $A_{\min}$.

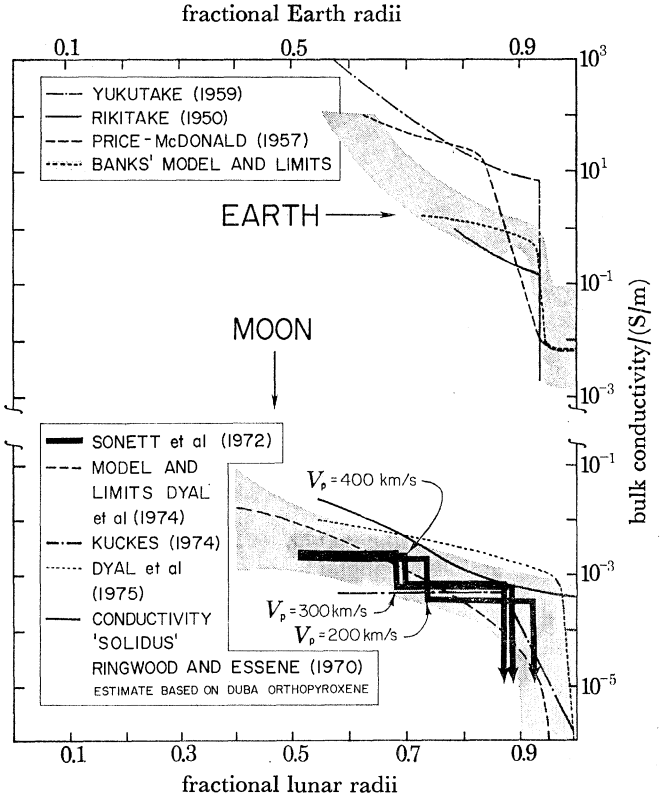

FIGURE 4. Comparative Earth and Moon conductivity profiles for several different investigators. The lunar data is extended from figure 2 in the following way. The 3L model is used and includes the effect of varying V_p. The Ringwood–Essene 'solidus' is derived by converting their solidus to equivalent conductivity using the Red Sea olivine (Duba *et al.* 1974).

There is strong evidence that plasma is present in all regions of the lunar orbit, but the solar wind pressure is screened away in the cavity and tail. Higher order induction restricts the present provisional conductivity profiles. The role of diamagnetism is unresolved; though an early argument suggested that for sunward data it cannot be due to ions as these are super-magnetosonic. A diagmanetic correction would decrease the conductivity estimate for the front side of the Moon. Kuckes (1974) uses an arbitrary estimate of $A_{\text{dia.}} = 0.2$ on the front side and this may account for his low conductivity estimate. However his $A_{\text{dia.}}$ is *ad hoc* and independent of frequency.

4. Estimates of the lunar temperature

Estimates of the internal temperature profile of the Moon have been reported by many workers based both upon time series and power spectral density derived conductivity profiles (Duba & Ringwood 1973; Dyal *et al.* 1972, 1974; Sonett *et al.* 1972; Sill 1972; Van'yan 1973, 1974). All of these are compositionally model dependent. The usual procedure is to use the suite of basic to ultrabasic silicate minerals, i.e. olivines and pyroxenes for the compositional model. The starting procedure uses a compositionally homogeneous Moon, but anomalies in the temperature may be found which then infer a variable compositional structure.

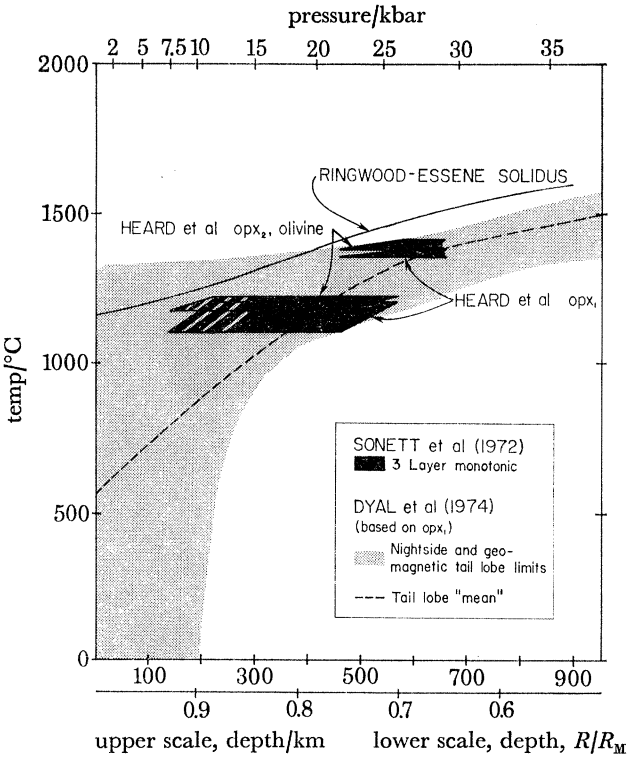

FIGURE 5. Temperature estimates for the Moon using the Red Sea olivine (Duba *et al.* 1974) and the Bamle enstatite (Heard *et al.* 1975) together with the 3L monotonic conductivity model with varying V_p, implying a variation in the admixture of quadrupole excitation. Both estimates lie close to the Ringwood–Essene solidus. (From Sonett & Duba 1975.) (From *Nature, Lond.* **258**, 118, 1975.)

Orthopyroxene-opx$_1$†: $\sigma_0 = 3 \times 10^7$ S/m; $\epsilon = 3.32$ eV for I/T $< 6.25 \times 10^{-4}$; $\sigma_0 = 2.03$ S/m; $\epsilon = 1.05$ ev for I/T $< 6.25 \times 10^{-4}$. Orthopyroxene-opx$_2$†: as above for I/T $< 6.25 \times 10^{-4}$; $\sigma_0 = 3.49$ S/m; $\epsilon = 1.14$ ev for I/T $< 6.25 \times 10^{-4}$. Olivine Fo(91): from Duba *et al.* 1974; $\sigma_0 = 17.4$ S/m; $\epsilon = 1.34$ below $T = 1320$ °C.

† Heard *et al.* (1975).

From considerations of resolution based upon Backus–Gilbert calculations (Schubert, private communication) the conductivity is likely unknown below a depth of about 800 km and at depth shallower than about 150–200 km. The published conductivity profiles of Dyal *et al.* (Dyal & Parkin 1973; Dyal *et al.* 1972, 1974) are continuous and cover a wide span in depth. Resolution tests of time series data are not available to this writer so that the justification for the quoted restrictions on depth are based solely upon test performed upon the iterated p.s.d. derived conductivity. A suggested concommittant resolution restriction upon time series (transients) can be based upon the heuristic observation that the quantity of data processed for

power spectral densities is at least as great *in total time extent* as for transient analysis. The qualitative conclusion is that the relative statistical limitations of transient analysis should at least equal that from p.s.d.

Because of limitations of this review we shall discuss in detail only the recent thermal inferences of Sonett & Duba (1975) derived from the 3L (Sonett *et al.* 1972) profile combined with the latest laboratory measurements on olivine (Duba *et al.* 1974) and Bamle enstatite (Heard *et al.* 1975). The results shown in figure 5 indicate little effect in substituting between olivine and pyroxene. The trapezoidal figures are the range of temperatures and shell radii from varying V_p, with fixed θ. The oxygen fugacity of the laboratory measurements was 10^{-8} bar (10^{-3} Pa), somewhat higher than expected for the Moon. The laboratory conductivity determinations exhibit a minimum at $f_{O_2} = 10^{-8}$ bar (Shankland 1975). The estimated temperatures lie close to the Ringwood–Essene (1970) solidus and are qualitatively consistent with the attenuation of the seismic shear wave which begins at about this depth (Toksoz *et al.* 1974; Nakamura *et al.* 1974). But the temperature estimates for the shell (of the 3L model) are inconsistent with mascon anisostasy (Arkani-Hamed 1973, 1974). Thus a compositional variation at the 150–200 km level in the Moon is suggested (Sonett *et al.* 1971*a*, *b*; Sonett & Duba 1975). This would not be especially surprising since this region is an enigmatic basalt source region candidate. Whether a bulk compositional change is actually required from the electromagnetic standpoint or whether merely a solid state dopant would suffice remains uncertain. Any valid solution to this problem should be consistent with geochemical constraints. There are, however, very wide since they are based upon a range of assumptions regarding the original bulk composition of the Moon. Also current fractionation models for the lunar mantle are variable and the degree of refinement required to explain the composition from the electrical data is not available, since the properties of mineral assemblages under lunar evolutionary constraints is poorly understood; this is true for electrical properties of rock in general.

The conclusion that the temperature at a depth of 450–600 km is high, although consistent with the seismic shear wave data, could be reduced if the rock conductivity is higher there than estimated from olivine/pyroxene. For example a small addition of H_2O could account for the wave damping and at the same increase the conductivity. If so a lower temperature would result and still be consistent with both types of data. However recent work on subsolidus convection suggests a temperature range consistent with our provisional results (Schubert *et al.* 1975*a*, *b*). Again these could lead to a lower temperature because of the effect of H_2O in depressing the viscosity function which, for lavas on Earth, is known to have a profound effect upon viscosity.

Sonnett & Duba (1975) also compare the thermal gradient with the data of Langseth *et al.* 1972; using the olivine/pyroxene temperature estimate at 150–200 km depth, the thermal gradient agrees with that derived using the heat flow data (Langseth *et al.* 1972), but the calculation is primitive, assuming heat sources not accumulated towards the surface. With the conflict inherent in the mascon rigidity requirement, it seems that a depression of the temperature estimate may be required. Then the thermal gradient should be reduced by about a factor of two. A high concentration of radionuclides near the surface is a lossy source of deep heating as most of the heat flux is conducted to the surface. Thus a high heat flux would be measured by the interior thermal gradient still be depressed.

PHILOSOPHICAL TRANSACTIONS OF THE ROYAL SOCIETY A MATHEMATICAL, PHYSICAL & ENGINEERING SCIENCES

(5) THE ATTAINMENT OF DEEP SOUNDING AND DETECTION OF A LUNAR CORE

Explaining the source of permanent magnetization of lunar rocks is a most enigmatic problem in current lunar science. If attributed to an ancient dynamo, the consequences are profound for Earth–Moon dynamics, the origin of the Moon, and for the thermal history. Density and axial moment of inertia (C/MR^2) arguments limit the possible radius of an Fe core to 450 km (Toksoz *et al.* 1974; Kaula *et al.* 1974) or to even 350 km if a larger value of C/MR^2 is assumed (Allen 1973). For an Fe/FeS core (Brett 1973) a radius of 700 km is suggested. It is straightforward to show that either type of core would be a nearly perfect reflector of very low frequency induced magnetic fields; the intensity of the transfer function and its shape at very low frequency could permit detection of a core as shown next.

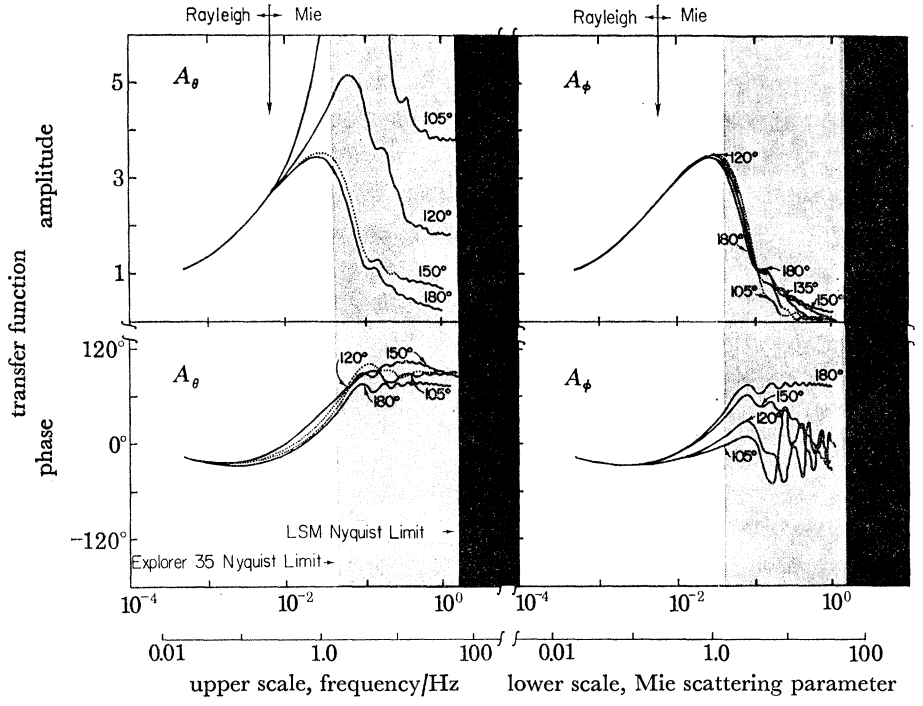

FIGURE 6. Transfer functions based upon s.s.p. theory for a 3L Moon with a superimposed core of varying conductivity. Cores of 1000, 700, 500 and 300 km are shown. The heavy boundary lines for each core size encompasses a suite of conductivities ranging from 10^{-2} to 10^{2} S/m. The perfect reflectivity of 10^{2} S/m cores is indicated by the asymptotic response at very low frequency.

The test calculations shown in figure 6 are based upon assumption of the standard 3L model of Sonett *et al.* (1972). In this model the Moon is assumed electrically homogeneous below about 1200 km, the depth depending upon the exact assumptions regarding quadrupole contributions to the field. This is equivalent to poor understanding of the Moon's conductivity below this depth using current data. The calculations are based upon s.s.p. theory. Asymmetric theory including cavity response gives identical results at extremely low frequency. However the 3L Moon can be combined with a core at greater depth to test core detection frequency and accuracy requirements. For this purpose we employ core radii of 1000, 700, 500 and 300 km with conductivities ranging upwards from 10^{-2} to 10^{2} S/m (for the 700 and 1000 km cases) and 10^{3} S/m for the 300 and 500 km cases. Figure 6 shows calculated gain functions G (§ 2) for the complete suite of core parameters, the heavy lines indicating outer limits.

The basic 3L Moon with 'isoconductive' interior has a gain function well decoupled from the core response permitting an approximate linear superposition of gain functions. For high conductivity limits each sized core approaches perfect reflectivity with the gain curve becoming constant as frequency drops. The asymptotic amplitude is a function of the distance of the core surface distance, the decrease in amplitude with core radius representing the nominal free space attenuation of a dipole. Figure 6 also shows the low conductivity limits for each of the four core sizes. All but the 1000 km core approximate the asymptotic 'no-core' limit of the 3L model. The 1000 km core represents a fourth shell, i.e. 4L model and is not accurately decoupled from the 3L model.

The conclusions to be drawn from figure 6 is the extreme frequency limit ($\sim 10\ \mu$Hz) required for core detection. Nominal 6/T data strips would imply $T = 6$ day swath lengths for p.s.d. processing. Such lengths are not available without significant gaps introduced by the Explorer 35 telemetry occultation of 0.5–2 h duration each 11.5 h. The statistical accuracy required is of order 1 % for 300 km core detection and somewhat less for a larger core.

Some very provisional data indicated by crossed bars has been taken from a set of 10 h swaths in figure 6. The conservative base frequency is taken to be $6/T$ where $T = 3.6 \times 10^4$ s so that $f_0 = 160\ \mu$Hz. These data show no evidence for a 'core' of radius 1000 km. Such a core should be construed selenophysically to first order in modelling as due to a continuing rise in temperature, although a compositional effect could also be present. The conductivity profile of Dyal *et al.* (1975) using tail lobe data, suggests that at 1000 km, the conductivity is order 2.2×10^{-2} S/m. A conductivity this large cannot be ruled out in figure 6 but is about 1.5 standard deviations away from the data mean. A core of 700 km radius is 1 standard deviation away from the data, and therefore convincing evidence for it is not present either. Indeed the data suggest a lunar interior relatively uniform in conductivity to a depth of 700 km. These comments are provisional, and will be revised using longer data swaths with appropriate contamination guards. An Fe core of radius less than about 700 km is completely uncertain and only requirements upon the data parameter limits can presently be given.

More recent work suggests that there is no evidence for a metallized core with a radius of 500 km or larger suggesting the absence of a Fe/FeS core of that radius. There is some suggestion in the new data of a second forcing function acting upon the Moon. This is hypothesized to be due to time variations of the diamagnetic field in the lunar cavity. Because of this some would tend to depress the main functions for those reported. Lastly, the data of figure 6 showing the two data points with large error bars have been revised upward by removal of data swaths near to the lunar terminator where it is suspected that confinement of the induced field tends to break down.

The work reported in this paper reviews some empirical highlights and theory on lunar induction since the discovery of the effect in 1969. The work of Schubert, Schwartz, Colburn and Smith is embedded throughout, but I assume responsibility for all the statements as time was not available for a complete review by other members of the group. I thank my colleagues for their aid in assembling the material reported herein. This work was supported by grant NSG 7020 from the Lunar Programs Office of N.A.S.A.

PHILOSOPHICAL TRANSACTIONS OF THE ROYAL SOCIETY A MATHEMATICAL, PHYSICAL & ENGINEERING SCIENCES

References (Sonett)

Allen, C. W. 1973 *Astrophysical quantities*. London: Athlone Press.

Arkani-Hamed, J. 1973 *The Moon* **6**, 100, 112–124.

Arkani-Hamed, J. 1974 *Proc. 5th Lunar Sci. Conf., Geochim. cosmochim. Acta Suppl.* 5, **3**, 3127–3134.

Brett, E. 1973 *Geochim. cosmochim. Acta* **37**, 165–170.

Duba, A., Heard, H. C. & Schock, R. N. 1974 *J. geophys. Res.* **79**, 1667–1673.

Duba, A. & Ringwood, A. E. 1973 *The Moon* **7**, 356–376.

Dyal, P. & Parkin, C. W. 1973 *Phys. Earth Planet. Int.* **7**, 251–265.

Dyal, P., Parkin, C. W. & Cassen, P. 1972 *Proc. 3rd Lunar Sci. Conf., Geochim. cosmochim. Acta Suppl.* **3**, **3**, 2287–2307.

Dyal, P., Parkin, C. W. & Daily, W. D. 1974 *Proc. 5th Lunar Sci. Conf., Geochim. cosmochim. Acta Suppl.* 5, **3**, 3059–3071.

Dyal, P., Parkin, C. W. & Daily, W. D. 1975 *Proc. 6th Lunar Sci. Conf.*, Houston (in the press).

Heard, H. C., Duba, A., Piwinski, A. J. & Schock, R. N. 1975 *Lunar Sci.* **6**, 355.

Kaula, W M , Schubert, G , Lingenfelder, R E., Sjogren, W. L. & Wollenhaupt, W. R. 1974 *Proc. 5th Lunar Sci. Conf., Geochim. cosmochim. Acta Suppl.* 5, **3**, 3049–3058.

Kuckes, A. F. 1974 *Nature, Lond.* **252**, 670–671.

Langseth, M. G., Jr, Clark, S. P., Jr, Chute, J. L., Jr, Keihm, S. J. & Wechsler, A. E. 1972 *The Moon* **4**, 390–410.

Nakamura, Y., Latham, G. B., Lammlein, D., Ewing, M., Duennebier, F. & Dorman, J. 1974 *Geophys. Res. Lett.* **1**, 137–140.

Ringwood, A. & Essene, E. 1970 In *Proc. Apollo* 11 *Lunar Sci. Conf., Geochim. cosmochim. Acta Suppl.* 1, **1**, 769–799.

Schubert, G. & Colburn, D. S. 1971 *J. geophys. Res.* **76**, 8174–8180.

Schubert, G. & Schwartz, K. 1972 *J. geophys. Res.* **77**, 76–83.

Schubert, G., Smith, B. F., Sonett, C. P., Colburn, D. S. & Schwartz, K. 1973 *J. geophys. Res* **78**, 3688–3696.

Schubert, G., Smith, B. F., Sonett, C. P., Colburn, D. S. & Schwartz, K. 1974 *Science, N.Y.* **183**, 1194–1196.

Schubert, G., Sonett, C. P., Smith, B. F., Schwartz, K. & Colburn, D. S. 1975*a* *Geophys. Res. Lett.* **2**, 277–280.

Schubert, G., Young, R. E. & Cassen, P. 1975*b* *Phil. Trans. R. Soc. Lond.* (in the press).

Shankland, T. J. 1975 *Phys. Earth Planet. Int.* **10** (in the press).

Sill, W. R. 1972 *The Moon* **4**, 3–17.

Sonett, C. P., Colburn, D. S., Dyal, P., Parkin, C. W., Smith, B. F., Schubert, G. & Schwartz, K. 1971*a* *Nature, Lond.* **230**, 359–362.

Sonett, C. P. & Duba, A. 1975 Submitted to *Nature, Lond.*

Sonett, C. P., Dyal, P., Parkin, C. W., Colburn, D. S., Mihalov, J. D. & Smith, B. F. 1971*b* *Science, N.Y.* **172**, 256–258.

Sonett, C. P., Smith, B. F., Colburn, D. S., Schubert, G. & Schwartz, K. 1972 In *Proc. 3rd Lunar Sci. Conf., Geochim. cosmochim. Acta Suppl.* 3, **3**, 2309–2336.

Toksoz, M. N., Dainty, A. M., Solomon, S. C. & Anderson, K. R. 1974 *Rev. Geophys. Space Phys.* **12**, 539–567.

Van'yan, L. L. 1973 *Ann. Geophys.* **29**, 367–374.

Van'yan, L. L. 1974 *Cosmic Res.* **11**, 823–824.

Wolfe, J. H., Mihalov, J. D., Collard, H. R., McKibbin, D. D., Frank, L. A. & Intriligator, D. S. 1974 *J. geophys. Res.* **79**, 3489–3500.

PHILOSOPHICAL TRANSACTIONS OF THE ROYAL SOCIETY A MATHEMATICAL, PHYSICAL & ENGINEERING SCIENCES

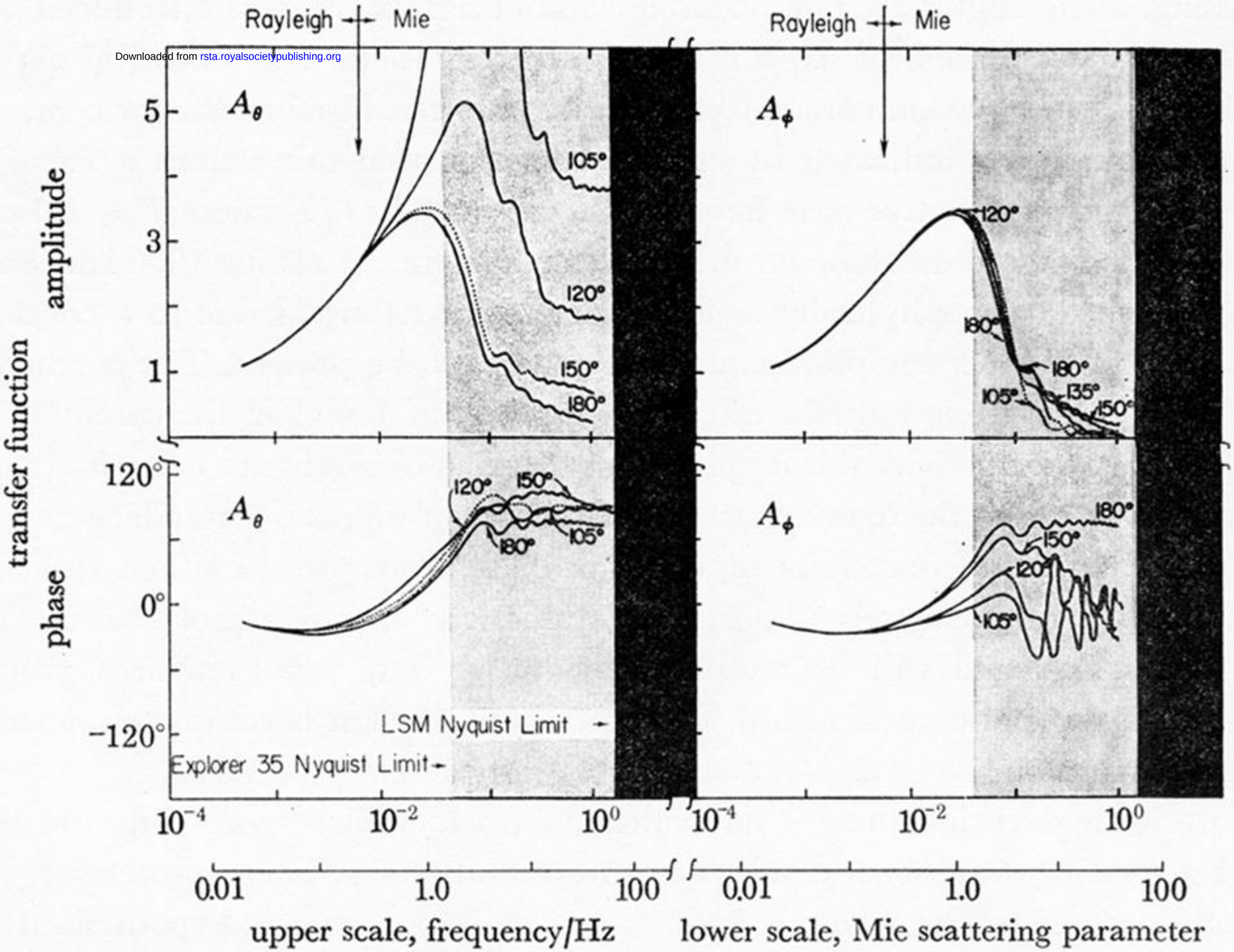

FIGURE 6. Transfer functions based upon s.s.p. theory for a 3L Moon with a superimposed core of varying conductivity. Cores of 1000, 700, 500 and 300 km are shown. The heavy boundary lines for each core size encompasses a suite of conductivities ranging from 10^{-2} to 10^{2} S/m. The perfect reflectivity of 10^{2} S/m cores is indicated by the asymptotic response at very low frequency.